Research Square

Preprints are preliminary reports that have not undergone peer review.
They should not be considered conclusive, used to inform clinical practice,
or referenced by the media as validated information.

Single Photon Reflection from a Quantum Dot in a Waveguide

Tarun Patel

t24patel@uwaterloo.ca

University of Waterloo

Matteo Pennacchietti

University of Waterloo

Sayan Gangopadhyay

University of Waterloo

Dan Dalacu

National Research Council of Canada

Philip Poole

National Research Council of Canada https://orcid.org/0000-0001-5163-7640

Stephen Hughes

Queen's University https://orcid.org/0000-0002-5486-2015

Michael Reimer

University of Waterloo

Physical Sciences - Article

Keywords:

Posted Date: April 2nd, 2026

DOI: https://doi.org/10.21203/rs.3.rs-8979997/v1

License: This work is licensed under a Creative Commons Attribution 4.0 International License.
Read Full License

Additional Declarations: There is **NO** Competing Interest.

Single Photon Reflection from a Quantum Dot in a Waveguide

Tarun Patel[1,2*†], Matteo Pennacchietti[1,2†], Sayan Gangopadhyay[2,3], Dan Dalacu[4,5], Philip J. Poole[4], Stephen Hughes[5], Michael E. Reimer[1,2,3*]

[1]Department of Electrical and Computer Engineering, University of Waterloo, Waterloo, N2L 3G1, Ontario, Canada.
[2]Institute for Quantum Computing, University of Waterloo, Waterloo, N2L 3G1, Ontario, Canada.
[3]Department of Physics and Astronomy, University of Waterloo, Waterloo, N2L 3G1, Ontario, Canada.
[4]National Research Council Canada, Ottawa, K1A 0R6, Ontario, Canada.
[5]Department of Physics, Engineering Physics and Astronomy, Queen's University, Kingston, K7L 3N6, Ontario, Canada.

*Corresponding author(s). E-mail(s): t24patel@uwaterloo.ca;
†These authors contributed equally to this work.

Abstract

Single-atom waveguide-QED systems have emerged as a leading platform for demonstrating non-linear optics in the few-photon regime [1–5]. Devices with such non-linear behavior are necessary for developing deterministic gates for photonic quantum computing [6, 7]. Artificial atoms coupled to nanophotonic or superconducting waveguides can be used to engineer highly efficient light-matter interfaces for such non-linear interactions, where every photon in the system interacts with the quantum emitter [8, 9]. However, it has been a challenge to access the reflection port of the waveguide due to the inability of rejecting stray electromagnetic fields that do not interact with the artificial atom [10, 11]. Here, we show coherent reflection of single photons from a semiconductor quantum dot strongly coupled to the fundamental waveguide mode of a nanowire. We utilize the tapered end of the nanowire for ideal mode-matching in a vertical geometry,

enabled by a novel extinction technique. This mode-matching allows for efficient transfer of photons from the input to the reflection port while having all interacted with the quantum dot. Such a high-efficiency scalable photonic platform opens up applications in few-photon quantum nonlinear optics and has been proposed for creating key resource states for universal photon-based quantum computing [12–15].

Introduction

Resonance fluorescence, where a single two-level system (TLS) is irradiated with monochromatic light, has fascinated physicists for more than a century. Its non-linear quantum mechanical behavior is evident in the fact that the TLS can only scatter a single photon at a time. The consequence of this, known as photon antibunching, was predicted by Carmichael and Walls [16] and observed by Kimble et al. in the fluorescence from sodium atoms [17]. It was envisioned by Kimble et al. that a TLS coupled strongly to a single electromagnetic mode could be used for deterministic photon-photon interactions [6, 18, 19]. Since then, it has been an outstanding challenge to couple a TLS to a single spatial electromagnetic mode. Originally, it was assumed that an optical dipole, which has a scattering cross-section of $\sigma = \frac{3\lambda^2}{2\pi}$, can be spatially matched with a focused Gaussian spot. However, more than 25 years ago, Enk and Kimble showed that most of the input light will not interact with the TLS in such an optical setup [20]. This weak coupling of the dipole with light is due to a non-uniform electric field distribution in the near-field of a tightly focused Gaussian spot. Soon after, Domokos et al. [8] proposed a solution to overcome this coupling problem by envisioning a TLS strongly coupled to a waveguide such that the spatial extent of the confined waveguide mode is comparable to the TLS scattering cross-section. In contrast to a focused Gaussian spot, a waveguide does not suffer from beam divergence and has a uniform k-space distribution along its optical axis. Thus, in such systems, strong waveguide-TLS coupling can be achieved. In this strong coupling regime, the

emission of the TLS is confined to a one-dimensional electromagnetic guided mode, thus forming a 'one-dimensional atom'.

In a one-dimensional atom, all of the incident electromagnetic field is perfectly reflected off the TLS when treated as a classical oscillating dipole in the ideal limit with no additional dephasing processes [21]. In the quantum regime, the quantized nature of the TLS restricts it to reflect only one photon per radiative lifetime. Alternatively, multiphoton states are transmitted through the one-dimensional atom [10, 22], analogous to a beamsplitter that sorts an input state based on its photon number. These processes are illustrated in Figure 1a, where we show a quantum trajectory (QT) simulation for a resonant coherent drive incident on an ideal waveguide-TLS system. Quantum jumps to the ground state (marked by green triangles) indicate a reflected single photon. In contrast, a quantum jump marked by the orange triangles implies a photon in the transmission port. As illustrated, two reflection events do not occur within the TLS lifetime, while a transmitted photon is always accompanied by a second photon emission into the reflection or transmission port. This effect in the classical limit was first observed in superconducting circuits by measuring near-perfect extinction of the incident electromagnetic field in the transmission port [23]. To demonstrate the quantum nature of the scattered field in the waveguide, autocorrelation measurements were performed in a later experiment showing antibunching in the reflection port and bunching in the transmission port. However, until now, it has been technically difficult to access the reflection port of the waveguide in a clean manner (i.e., without stray electromagnetic fields that have not interacted with the TLS backscattering into the reflection port). This is evident in previous results as even though the $g^{(2)}(0)$ was sub-Poissonian, it was limited to 0.6 [11].

In this work, we measure resonant reflection from a semiconductor quantum dot strongly coupled to a nanophotonic waveguide in the Heitler regime. In this regime, it has been well established that the resonant fluorescence spectrum in the weak drive

limit of a TLS is coherent with the excitation [24–26]. Mainly, we establish near-unity mode-matching to the nanowire waveguide, obtaining clean access to the reflection port of the one-dimensional atom for the first time. Since the quantum dot is strongly coupled to the fundamental waveguide mode, we show that all the back-scattered light can be treated as reflection off the TLS. Using this novel mode-matching technique, we demonstrate single photon reflection off the TLS by measuring antibunching with a $g^{(2)}(0)$ of 0.025. Combining this antibunching of $g^{(2)}(0) < 0.5$, and the coherent nature of the reflected light, we realize a 'quantum mirror' in our experiment. This *quantum mirror* effect disappears with increasing number of incident photons within the radiative lifetime as the TLS is continuously saturated and its emission becomes incoherent with respect to the drive. Such non-linear behaviour has long been sought after for the development of deterministic gates in photonic quantum computing and quantum networks.

Mode-matching to the Nanowire Quantum Dot

We realize our waveguide-TLS with a single InAsP quantum dot located on the axis of a cylindrical InP nanowire waveguide. The waveguide-quantum dot system is grown in a site-selected manner by chemical beam epitaxy using vapour-liquid-solid and selective-area growth. The growth parameters can be tuned to achieve precise control over the waveguide and quantum dot dimensions [27]. To achieve strong coupling between the nanowire waveguide and the TLS, the waveguide mode cross-section must be comparable to the scattering cross-section of the TLS [8]. This regime is achieved when at least half of the spontaneous emission from the TLS couples to the fundamental HE_{11} waveguide mode, defined as the β-factor. For our nanowire waveguide-quantum dot (NWQD) system, this condition is met for d/λ ranging from 0.17 to 0.33 [28, 29], where d is the effective diameter of the nanowire waveguide and λ is the emission wavelength of the TLS. The nanowires used in our experiments have a d/λ of $\sim$0.29, yielding a beta-factor of $\sim$ 90%.

Additionally, the nanowire waveguide is tapered adiabatically towards the tip with a tapering angle of $\sim 1^\circ$ as shown in the SEM image of Figure 1b. In Supplementary Note 2, we show the finite-difference time-domain (FDTD) simulations for a radiating dipole placed on the axis of the nanowire waveguide, modeled using the dimensions from Figure 1b. The taper ensures that the fundamental HE_{11} mode gradually expands from inside the nanowire to a free-space Gaussian propagating mode with minimal back-reflections. Previous studies have shown efficient coupling (∼93%) of the quantum dot emission to a single mode fiber from similar NWQD structures, confirming this Gaussian emission [30].

In this work, we focus on the efficient in-coupling of a free-space Gaussian light beam to the HE_{11} waveguide mode of the nanowire. First, we used FDTD simulations to model the in-coupling and determine the ideal in-coupling efficiency of 97%. Supplementary Figure 3a shows the evolution of the electric field for an incident focused Gaussian beam on the tapered nanowire waveguide under optimal mode-matching conditions. By leveraging the mode matching parameters, we design an optical system shown in Figure 1c. We choose a lens that collimates the input laser from a single-mode fiber (SMF) to have the same mode field diameter as the collimated NWQD emission from the objective lens. The input laser is reflected from a 93(T):3(R) non-polarizing beam-splitter into the objective lens inside a 4K cryostat and focused on the NWQD. The QD emission is then collected from the transmission port of the beam-splitter and coupled into a second SMF using a replica of the input collimating lens.

To determine the mode-field diameter of the QD emission at ∼895 nm, we measure its k-space distribution using a 4f-imaging setup (see Supplementary Figure 4 for details of the 4f-imaging setup) [30]. In Figure 2a, we show a typical emission profile of a NWQD, which has a 99% overlap with a 2D Gaussian corresponding to an NA of 0.30 (at $1/e^2$). To achieve efficient in-coupling to the nanowire, we shape the input mode to have a NA and wavelength similar to that of the output (see Methods). To

obtain optimal mode-matching conditions on the nanowire, the Gaussian spot needs to be focused $\sim$4 µm from the growth substrate (shown in Supplementary Figure 3a). We solve this challenge by monitoring the extinction pattern of the reflected laser in k-space. Here, we leverage the fact that the k-space image is invariant to translation of the focal point in the z-direction. This contrasts with the real-space image that defocuses sharply with any change in z. Full details of mode-matching in the z-direction is given in Supplementary Note 3. It is important to note that light coupled into the HE_{11} waveguide mode propagates through the NW and leaves the system through the zinc blende growth substrate. This transmission of the light through the system is observed as a reduction in the intensity (I) of the reflected light as compared to the Fresnel reflection off the planar substrate. Using the FDTD model discussed in Supplementary Note 2, we calculate the ideal magnitude of this extinction, E, to be 90% ($E = 1 - I_{NW}/I_{substrate}$).

In Figure 2b, we show the measured k-space image of the reflected light from the substrate (left panel) and under ideal mode-matching conditions on the nanowire (right panel) without changing the focal plane. We observe an angular distribution of the back-scattered light from the nanowire that matches qualitatively with the expected distribution shown in Supplementary Figure 3c. Quantitatively, we observe an average extinction of 86% for 10 nanowires as shown in the Supplementary Table 1. For the remainder of this work, we focus on a nanowire with an 85% extinction ratio under mode matching conditions. This close agreement between theory and experiment allows us to conclude that ***$\sim$95% of the input Gaussian beam is coupled to the HE_{11} waveguide mode***.

By combining the high in-coupling and out-coupling mode matching efficiencies, we effectively extend the reflection port of the NWQD-waveguide mode from 4K to room temperature. The high in-coupling efficiency and β-factor ensures that all the

input light interacts with the QD. Since the outcoupling SMF only couples to a Gaussian mode, the high NA components of the back-scattered/reflected light (Figure 2b right panel) are not collected. As a result, our NWQD system enables effective suppression of the input laser signal without the need for the well-known and utilized cross-polarization filtering technique for resonance fluorescence [31]. Remarkably, with our mode-matching technique, we can obtain ***robust resonance fluorescence from a TLS while only using spatial filtering enabled by our nanophotonic structure***.

Quantum Mirror

Resonance fluorescence in the Heitler regime has been observed previously to consist of elastically scattered photons from the TLS [25, 26]. Interestingly, in our NWQD system, all of the elastic scattering occurs into the reflection port, mimicking reflection off a mirror. Nonetheless, due to the quantized nature of the TLS, our 'mirror' can only reflect single photons at a time and is saturated when, on average, more than one photon arrives within its lifetime. We now verify the high efficiency of our optical setup and demonstrate this *quantum mirror* effect by comparing the modeled reflection from the NWQD to experimental results.

We model the resonance fluorescence from our one-dimensional atom using a master equation with an input-output formalism to include the influence of the waveguide on the quantum TLS (see Supplementary Note 1 for the mathematical treatment). To probe the reflection, we input coherent light on the excitation path, which is mode-matched to the NWQD. We then scan the wavelength of the input light across the exciton resonance and monitor the reflection port of the NWQD through the 93% transmission path of the optical setup (Figure 1c). The result of one such scan in the low power regime with an input laser power corresponding to a mean photon number $\langle n \rangle$ of 0.01 per QD lifetime is shown in Figure 3a. Using the parameters shown in the Supplementary Note 4, we modelled the expected response of the reflected intensity

(Supplementary Note 1) with $\langle n \rangle$ as the only free parameter. The fit estimates $\langle n \rangle$ to be 0.014, which is in close agreement with the measured value, thus validating the input parameters to our model. We note that these input parameters were obtained by separate measurements and simulations.

We find that the observed reflection exhibits Gaussian line broadening due to charge noise. A Voigt fit yields an inhomogeneous FWHM QD linewidth of 4.4 ± 0.6 GHz, which is >20x away from the Fourier-transform limit of 177 MHz (determined by radiative life-time measurements; see the Supplementary Figure 7). We note that a weak above-band laser onto the nanowire was needed to reduce charge noise and obtain a more stable response. We confirm that this above band laser does not introduce any additional luminescence to the reflected signal (see Supplementary Note 5 for details).

With an increasing incident $\langle n \rangle$, this perfect reflection from the NWQD saturates. This saturation effect is demonstrated in Figure 3b, where we plot the total reflected intensity normalized to the background (R_{int}) as a function of incident laser intensity given as $\langle n \rangle$ per QD lifetime. The background is defined as the intensity of light observed off-resonance and is interpreted to have not interacted with the NWQD. The blue data points are extracted from the fitted model to the NWQD reflection linewidth scans similar to Figure 3a. We measure the QD reflection response for seven decades of incident $\langle n \rangle$. The red line plots the expected R_{int} using parameters from the fit of Figure 3a where we now vary $\langle n \rangle$. We observe excellent agreement between the experimentally measured data points and the modeled response. As shown in Figure 3b, the reflected intensity, R_{int}, is constant for $\langle n \rangle$ ranging from 10^{-6} to 10^{-1} where the one-dimensional atom behaves as a perfect reflector of single photons. As $\langle n \rangle$ increases above 0.1, the probability of multiphoton components in the incident drive increases significantly, resulting in a drop of R_{int}.

To confirm the single photon reflection, we perform second-order correlation measurements on the reflected signal using a standard Hanbury-Brown and Twiss setup.

The results of these measurements for varying incident $\langle n \rangle$ are shown in Figure 4a. We observe an antibunching dip centred around zero-time delay with a width that is consistent with the measured spontaneous emission lifetime of the TLS. We emphasize that due to the precise mode matching of the light in and out of the nanowire waveguide, we obtain a low $g^{(2)}(0)$ of 0.025 for an incident $\langle n \rangle$ of 0.001 without any corrections. This confirms that the coupling into the reflection port of back-scattered laser light that did not interact with the TLS is heavily suppressed. This fact is evident in the $g^{(2)}(\tau)$ for an incident $\langle n \rangle = 1$, where we do not observe any degradation of the $g^{(2)}(0)$ signal compared to $\langle n \rangle$ of 0.001, while even for an $\langle n \rangle = 10$, the $g^{(2)}(0)$ is only 0.21.

We now turn our attention to the changing dynamics of the $g^{(2)}(\tau)$ response to increasing incident drive. At high drive ($\langle n \rangle = 10$), we observe side-bunching peaks within the spontaneous emission lifetime corresponding to fast Rabi oscillations of the TLS. The Rabi oscillations indicate the significant dressing of the TLS due to the input drive and the onset of the Mollow triplet.

As discussed previously, the majority of the reflected signal ($> 95\%$) consists of emission from the one-dimensional atom. We now study the spectral response of the reflected signal at resonance by resolving it using a Fabry-Perot etalon (see Methods) as shown in Figure 4b. In the Heitler regime, the emission from the TLS is dominated by coherent scattering in the weak drive limit. This is evident as the input drive power is reduced. At the highest input power of $\langle n \rangle = 10$, a significant amount of incoherent emission is observed when the measured intensity is plotted in log scale. We distinguish between the coherent and incoherent emission by overlaying the instrument response function (IRF, red curve) of the Fabry-Perot etalon with the data (colored dots). We attribute the part of the RF under the red curve as the coherent emission. Note that the actual coherent emission is on the order of the laser linewidth ($\sim$10 kHz), which is far below the IRF of 66 MHz. The remaining RF is attributed to incoherent emission.

As the input drive power decreases, the fraction of incoherent to coherent emission reduces according to $2(\Omega/\gamma)^2$, where Ω is the Rabi frequency and γ is the spontaneous emission rate. We emphasize that at low input drive power ($\langle n \rangle = 0.001$) we can no longer distinguish between the coherent and incoherent emission since a Voigt fit to the raw data gives a linewidth similar to the IRF.

Discussion

We now discuss the physical picture of the underlying dynamics of this single-photon reflection. In the low-power limit, the reflection port of the NWQD behaves analogous to an optical mirror, as the reflected signal has the same frequency and similar spectral linewidth to that of the excitation. Yet, despite this spectral overlap, the photon statistics of the reflected light are distinctly non-classical as observed in the second-order correlations. In our waveguide-QED system, the TLS at its resonant frequency imposes a π phase shift on the input drive, analogous to a driven classical harmonic oscillator. Due to the additional non-linear saturation of the TLS, this reflection is effectively limited to one photon per radiative lifetime [32], which leads to destructive interference of all multiphoton components in the detection channel of our experiment. This non-linearity imparts anharmonicity to the TLS and thus, the reflected field can be shown to be a displaced, squeezed vacuum state by perturbative expansion of the TLS response. Here, the photon antibunching in the reflection port is associated with self-homodyning of this squeezed fluorescence from the TLS [33]. We model the squeezing of our reflected signal, as shown in Supplementary Note 1, and note that pure dephasing reduces the squeezing considerably. However, we find that this reduction in squeezing does not affect the measured antibunching. Alternatively, the NWQD can also be thought of as capable of reflecting photons spaced by its radiative lifetime, but if two photons arrive within its lifetime, one photon will be transmitted while the TLS is busy interacting with the other photon [32] as shown by the QT plot in Figure 1a. The contrast between these continuous (time-independent)

and discrete pictures has led to recent fruitful debates and is being exploited for creating new forms of non-classical light by multi-photon engineering of resonance fluorescence from bulk quantum dots [34]. Our NWQD waveguide-QED system provides a nanophotonic platform whereby non-linear photon transport is efficiently confined to a single spatial mode such that every photon in the system can be accounted for. Thus, our novel mode-matching technique enables efficient access to non-linear quantum optics at the few-photon level in a scalable nanophotonic platform.

Summary

By near-perfect mode matching into a photonic nanowire quantum dot system, we have shown the first demonstration of clean single-photon reflection from a one-dimensional atom where we measure a raw $g^{(2)}(0)$ of 0.025 without cross-polarized laser suppression. We verified the high ($\sim$95%) in- and out-coupling from the NWQD by achieving close agreement between our model and experimentally measured reflected intensity and second-order correlations as a function of input drive. Finally, we confirmed that the coherence of the reflected signal is comparable to the excitation as the input drive is reduced. Thus, the NWQD photonic system is an ideal platform for generating bright sources for such non-classical states of light, which are required for practical implementations of engineering photon statistics for photonic quantum information processing and networks [34–36]. For such applications obtaining Fourier-limited linewidths is critical and will require electrostatic control over the charge environment around the quantum dot. Furthermore, the transmission port of the NWQD can be easily accessed through the transparent growth substrate and will enable complete access to the photon dynamics of our waveguide QED system [10].

Future work on this platform can now focus on the study of non-Markovian dynamics of quantum systems. Such experiments require excitation of the TLS with antibunched light, which can be realised in our NWQD system with delayed coherent feedback by rerouting the resonance fluorescence of the TLS back to itself [37].

Alternatively, on-demand single-photon sources are now reaching maturity and thus can also be used for non-classical excitation of the TLS. We envision that our system will enable access to few photon nonlinearities to realize single-photon waveplates [18] and photon-photon gates [6, 7], as originally proposed by Kimble.

Acknowledgments. We acknowledge Lennart Jehle for assisting with the k-space imaging setup and Sarah Odinotski for the SEM image of the NWQD. We would also like to acknowledge Robin Williams for motivating this project.

Declarations

- Funding: M.E.R. would like to acknowledge financial support from NSERC Quantum Alliance, NSERC Discovery, and NRC Quantum Sensing Program, which funded part of this research. S.H. thanks NSERC Quantum Alliance, NSERC Discovery, and Queen's University for funding.
- Conflict of interest/Competing interests: The authors declare no competing interests.
- Data availability: Available upon request.
- Code availability: The corresponding code for the w-QED model can be made available upon reasonable request from the corresponding author.
- Author contribution: M.E.R. and T.P conceived and designed the experiments. T.P. and M.P. performed the experiments with input from M.E.R., S.G., D.D, and P.P. D.D. and P.P. grew the NWQD. S.G. performed numerical simulations with input from T.P. and M.P. S.G. and M.P. developed the theoretical model under the supervision of S.H. with input from T.P. T.P. and M.E.R. wrote the manuscript with input from all authors.

References

[1] Bhaskar, M. K. *et al.* Quantum nonlinear optics with a germanium-vacancy color center in a nanoscale diamond waveguide. *Phys. Rev. Lett.* **118**, 223603 (2017). https://doi.org/10.1103/PhysRevLett.118.223603.

[2] Chang, D. E., Sørensen, A. S., Demler, E. A. & Lukin, M. D. A single-photon transistor using nanoscale surface plasmons. *Nat. Phys.* **3**, 807–812 (2007). https://doi.org/10.1038/nphys708.

[3] Javadi, A. *et al.* Single-photon non-linear optics with a quantum dot in a waveguide. *Nat. Commun.* **6**, 8655 (2015). https://doi.org/10.1038/ncomms9655.

[4] Hoi, I.-C. *et al.* Demonstration of a single-photon router in the microwave regime. *Phys. Rev. Lett.* **107**, 073601 (2011). https://doi.org/10.1103/PhysRevLett.107.073601.

[5] Le Jeannic, H. *et al.* Dynamical photon–photon interaction mediated by a quantum emitter. *Nat. Phys.* **18**, 1191–1195 (2022). https://doi.org/10.1038/s41567-022-01720-x.

[6] Duan, L.-M. & Kimble, H. J. Scalable photonic quantum computation through cavity-assisted interactions. *Phys. Rev. Lett.* **92**, 127902 (2004). https://doi.org/10.1103/PhysRevLett.92.127902.

[7] Hacker, B., Welte, S., Rempe, G. & Ritter, S. A photon-photon quantum gate based on a single atom in an optical resonator. *Nature* **536**, 193–196 (2016). https://doi.org/10.1038/nature18592.

[8] Domokos, P., Horak, P. & Ritsch, H. Quantum description of light-pulse scattering on a single atom in waveguides. *Phys. Rev. A* **65**, 033832 (2002).

https://doi.org/10.1103/PhysRevA.65.033832.

[9] Shen, J. T. & Fan, S. Coherent photon transport from spontaneous emission in one-dimensional waveguides. *Opt. Lett.* **30**, 2001–2003 (2005). https://doi.org/10.1364/ol.30.002001.

[10] Le Jeannic, H. *et al.* Experimental reconstruction of the few-photon nonlinear scattering matrix from a single quantum dot in a nanophotonic waveguide. *Physical review letters* **126** (2021).

[11] Hoi, I.-C. *et al.* Generation of nonclassical microwave states using an artificial atom in 1D open space. *Physical Review Letters* **108**, 263601 (2012).

[12] Pichler, H., Choi, S., Zoller, P. & Lukin, M. D. Universal photonic quantum computation via time-delayed feedback **114**, 11362–11367. https://doi.org/10.1073/pnas.1711003114.

[13] Chang, D. E., Vuletić, V. & Lukin, M. D. Quantum nonlinear optics — photon by photon **8**, 685–694. https://doi.org/10.1038/NPHOTON.2014.192.

[14] Zheng, H., Gauthier, D. J. & Baranger, H. U. Waveguide-QED-based photonic quantum computation. *Phys. Rev. Lett.* **111**, 090502 (2013). https://doi.org/10.1103/PhysRevLett.111.090502.

[15] Yang, F., Lund, M. M., Pohl, T., Lodahl, P. & Mølmer, K. Deterministic photon sorting in waveguide QED systems **128**, 213603. https://doi.org/10.1103/PhysRevLett.128.213603.

[16] Carmichael, H. J. & Walls, D. F. A quantum-mechanical master equation treatment of the dynamical stark effect. *J. Phys., B Proc. Phys. Soc., At. Mol. Phys.* **9**, 1199–1219 (1976).

[17] Kimble, H. J., Dagenais, M. & Mandel, L. Photon antibunching in resonance fluorescence. *Phys. Rev. Lett.* **39**, 691 (1977). https://doi.org/10.1103/PhysRevLett.39.691.

[18] Turchette, Q. A., Hood, C. J., Lange, W., Mabuchi, H. & Kimble, H. J. Measurement of conditional phase shifts for quantum logic. *Phys. Rev. Lett.* **75**, 4710–4713 (1995).

[19] Tomm, N. *et al.* Realization of a coherent and efficient one-dimensional atom. *Phys. Rev. Lett.* **133**, 083602 (2024).

[20] van Enk, S. J. & Kimble, H. J. Strongly focused light beams interacting with single atoms in free space. *Phys. Rev. A* **63**, 023809 (2001). https://doi.org/10.1103/PhysRevA.63.023809.

[21] Zumofen, G., Mojarad, N. M., Sandoghdar, V. & Agio, M. Perfect reflection of light by an oscillating dipole. *Phys. Rev. Lett.* **101**, 180404 (2008). https://doi.org/10.1103/PhysRevLett.101.180404.

[22] Hallett, D. *et al.* Electrical control of nonlinear quantum optics in a nano-photonic waveguide. *Optica* **5**, 644–650 (2018).

[23] Astafiev, O. *et al.* Resonance fluorescence of a single artificial atom. *Science (New York, N.Y.)* **327**, 840–843 (2010).

[24] Heitler, W. *The Quantum Theory of Radiation* 3 edn (Oxford University Press, New York, 1954).

[25] Matthiesen, C., Vamivakas, A. N. & Atatüre, M. Subnatural linewidth single photons from a quantum dot. *Physical review letters* **108**, 093602 (2012).

[26] Hanschke, L. *et al.* Origin of antibunching in resonance fluorescence. *Physical review letters* **125**, 170402 (2020).

[27] Laferrière, P. *et al.* Unity yield of deterministically positioned quantum dot single photon sources. *Scientific reports* **12**, 6376 (2022).

[28] Claudon, J., Gregersen, N., Lalanne, P. & Gérard, J.-M. Harnessing light with photonic nanowires: fundamentals and applications to quantum optics **14**, 2393–2402. https://doi.org/10.1002/cphc.201300033.

[29] Dalacu, D., Poole, P. J. & Williams, R. L. Nanowire-based sources of non-classical light. *Nanotechnology* **30**, 232001 (2019). https://doi.org/10.1088/1361-6528/ab0393.

[30] Bulgarini, G. *et al.* Nanowire waveguides launching single photons in a Gaussian mode for ideal fiber coupling **14**, 4102–4106. https://doi.org/10.1021/nl501648f.

[31] Kuhlmann, A. V. *et al.* A dark-field microscope for background-free detection of resonance fluorescence from single semiconductor quantum dots operating in a set-and-forget mode **84**, 073905. https://doi.org/10.1063/1.4813879.

[32] Carmichael, H. J. Quantum trajectory theory for cascaded open systems **70**, 2273–2276. https://doi.org/10.1103/PhysRevLett.70.2273.

[33] Carmichael, H. *An Open Systems Approach to Quantum Optics* (Springer Berlin Heidelberg, 1993). http://dx.doi.org/10.1007/978-3-540-47620-7.

[34] Kim, S. K. *et al.* Unlocking multiphoton emission from a single-photon source through mean-field engineering **11**, eadw3395. https://doi.org/10.1126/sciadv.adw3395.

[35] Zubizarreta Casalengua, E., López Carreño, J. C., Laussy, F. P. & Valle, E. d. Conventional and unconventional photon statistics. *Laser Photon. Rev.* **14**, 1900279 (2020). https://doi.org/10.1002/lpor.201900279.

[36] Tomm, N. *et al.* Photon bound state dynamics from a single artificial atom. *Nat. Phys.* **19**, 857–862 (2023). https://doi.org/10.1038/s41567-023-01997-6.

[37] Crowder, G., Ramunno, L. & Hughes, S. Quantum trajectory theory and simulations of nonlinear spectra and multiphoton effects in waveguide-QED systems with a time-delayed coherent feedback. *Phys. Rev. A (Coll. Park.)* **106**, 013714 (2022). https://doi.org/10.1103/physreva.106.013714.

Methods

μ-PL Setup with mode-matching to a NWQD.

The NWQD sample was kept at 4.5K in an attoDRY 800 cryostat with an optical access window. A wedged CaF_2 window was used as a 93:3 (T:R) beamsplitter allowing for efficient collection on the reflection port.

A 3.1 mm focal length aspheric lens (LightPath 355330) housed inside the optical cryosat was used as the objective lens to mode-match into the NWQD and collect reflected fluorescence. The NWQD emission collimated by the aspheric lens has a mode field diameter of $NA_{NW}/NA_{obj} \times$Clear Aperature $= 0.30/0.77 \times 5\text{mm} = 1.96\,\text{mm}$. See Supplementary Note 6 for the fitted cross-section of the NWQD emission in k-space used to determine the NA of the NW. To match the MFD of the collimated NWQD emission, the drive laser is launched from a 780HP fiber with an aspheric lens of 11 mm focal length (Newport 5725-B-H) to create an MFD of $0.11/0.3 \times 5.5\,\text{mm} = 2.0$ at 885 nm. Similarly, the reflected fluorescence (transmitted through the beamsplitter)

is coupled into a second 780HP fiber using a second 11 mm Newport aspheric lens. A detailed account of the total system efficiency is described in Supplementary Table 2.

The drive laser used for resonant excitation was a Toptica CTL 900 external tunable diode laser with a nominal linewidth of 10kHz. The intensity of excitation to the NW is monitored by measuring the transmission through the beamsplitter using a calibrated silicon photodiode (Thorlabs S120C). The input drive intensity is controlled using a set of pre-calibrated absorptive neutral density filters and a half-wave plate with a polariser.

Fabry-Perot measurements

A Thorlabs (SA210-8B) scanning Fabry-Perot interferometer (FPI) was used to measure the linewidth of the reflected signal from the NWQD. The nominal free-spectral range (FSR) and finesse of the FPI are 10GHz and 180, respectively. A Qontrol Ltd. Q8iv programmable voltage source was used to drive the piezo actuators inside the FPI to scan a full FSR with a step size of 30 MHz. See Supplementary Note 7 for details on the measurement of the instrument response function of the FPI.

Single Photon Detection

All single photon detection was performed using Single Quantum superconducting nanowire single-photon detectors with $\sim 85\%$ detection efficiency at 900 nm and 14 ps timing jitter (FWHM).

Main Figures:

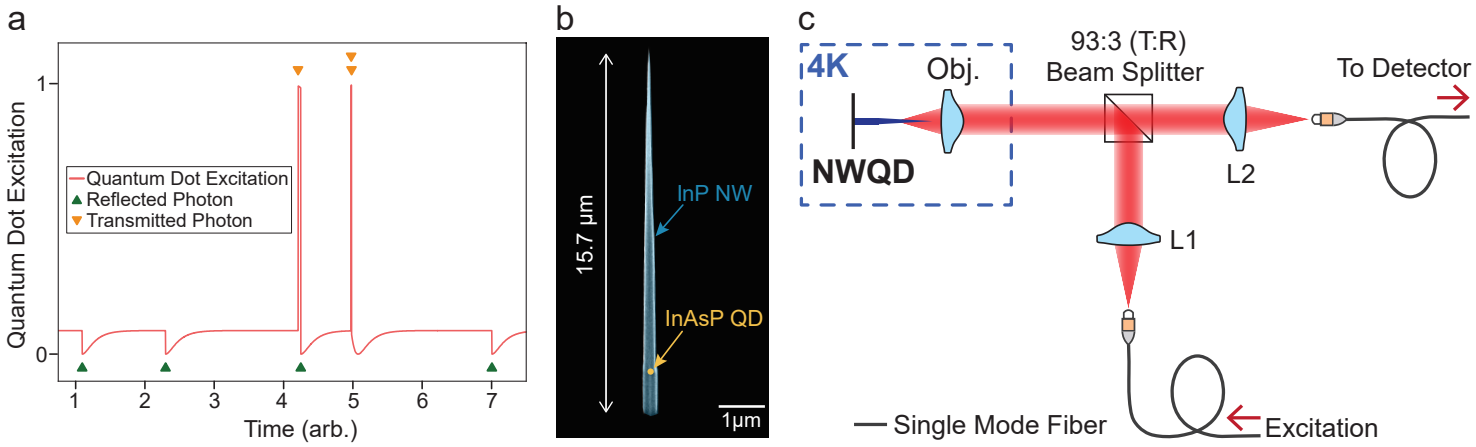


Fig. 1: **Waveguide-QED with a semiconductor quantum dot in a nanophotonic waveguide.** (a) Sample quantum trajectory in the weak-excitation limit of a single-atom waveguide-QED system. Photon detection events in the transmission and reflection ports are labeled with orange and green triangles, respectively. See Supplementary Note 1 for details. (b) False colored SEM image of the NWQD showing the InP nanowire waveguide with an adiabatic taper in blue and the nominal location of the InAsP quantum dot with a yellow circle. (c) Schematic of the experimental configuration for extending the waveguide mode of the NWQD in a 4K system to a room temperature single-mode fiber (780HP). The collimating/coupling lenses (L1 & L2) for the single-mode fiber are chosen to match the output mode of the NWQD after the collimating objective (Obj.). This mode-matching to the fundamental mode of the nanowire waveguide enables $\geq 90\%$ input and collection efficiencies of the reflection port.

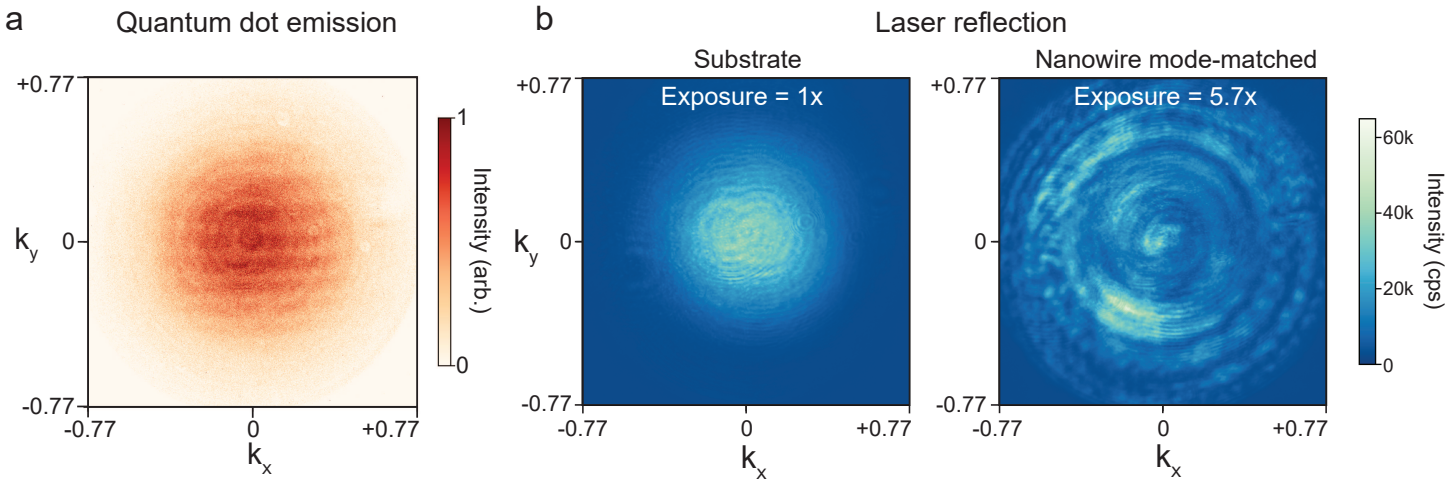


Fig. 2: **Establishing mode-matching to the nanowire quantum dot.** (a) K-space image of the quantum dot emission obtained using a 4f imaging system under above-bandgap excitation. The emission mode fits a Gaussian profile with an NA of 0.3, which is used to design the experimental setup shown in Figure 1c (see Methods). (b) K-space image of the reflected laser from the planar growth substrate (left) and the NWQD under ideal mode matching conditions (right) taken with 1x and 5.7x exposure times, respectively. The extinction of the Fresnel reflection of the input laser is used to monitor mode matching to the nanowire waveguide mode. The total intensity of the reflected signal on the right shows a reduction of 85% as measured using a power meter. Concentric rings observed under mode-matched conditions and the extinction value obtained are in good agreement with FDTD simulation results.

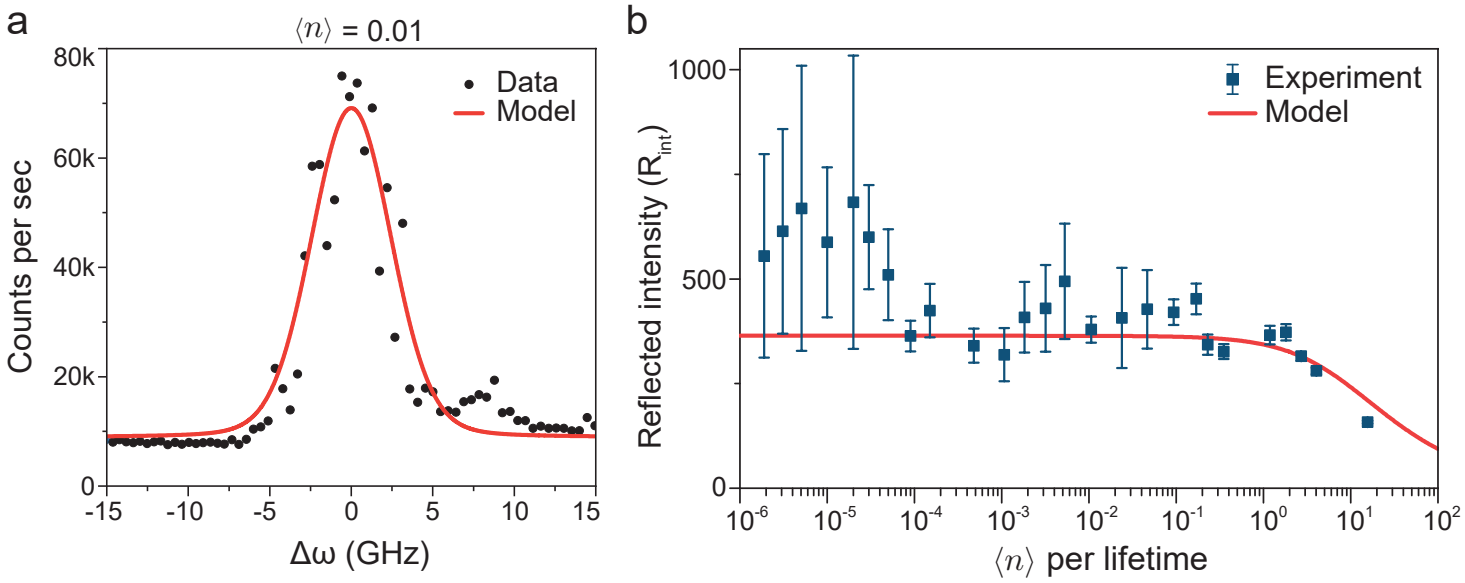


Fig. 3: **Resonant reflection from a quantum dot in a waveguide.** (a) Reflection from the NWQD as a function of detuning $\Delta\omega$ centred around the exciton resonance. Black dots show the experimental data with a measured input drive corresponding to an incident mean photon number $\langle n \rangle$ of 0.01. The expected response from the master-equation model is shown by the red line, which estimates the input drive to be $\langle n \rangle = 0.014$. A Voigt fit to the data (shown in SI) yields an inhomogeneous QD linewidth of 4.2 GHz. (b) Integrated reflected intensity R_{int}, obtained by integrating detuning scans similar to Figure 3a, as a function of $\langle n \rangle$ varied from 10^{-6} to 10. Blue squares with error bars are experimentally measured data points, and the red line shows the expected response determined from the parameters of the model used in Figure 3a. The single-photon reflection from the NWQD saturates as $\langle n \rangle$ exceeds 1 and is characterized by the expected drop in R_{int}. This reduction in R_{int} is also observed by the experimental data. We note that a higher R_{int} is measured compared to the model at lower drive power ($< 10^{-4}$), and is due to overestimating the background counts in the experiment.

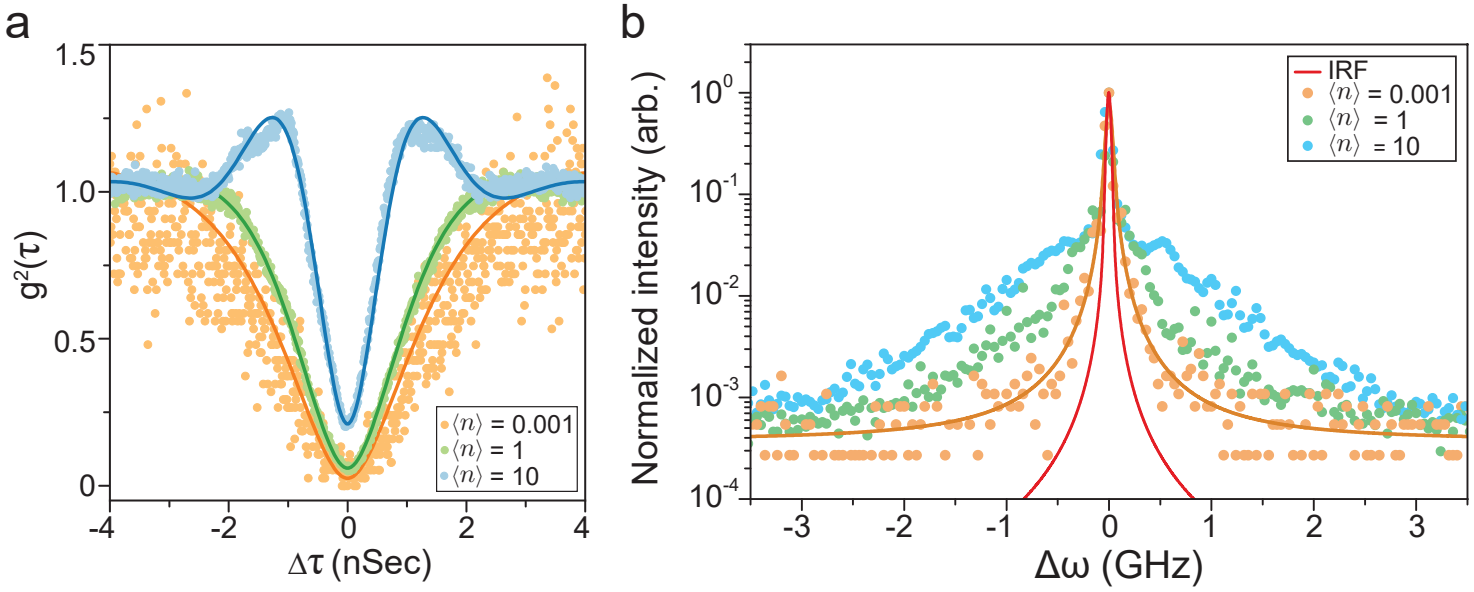


Fig. 4: **Coherent single-photon reflection in a waveguide-QED system.** (a) Second order correlation $g^{(2)}(\tau)$ and (b) coherence of the reflected signal for three input $\langle n \rangle$ of 0.001 (orange), 1 (green) and 10 (blue) respectively. (a) The $g^{(2)}(\tau)$ data is shown by colored dots while the modeled response is outlined by a solid line of the same color. The raw $g^{(2)}(0)$ for low $\langle n \rangle$ of 0.001 is 0.025, which remains below 0.5 for a significantly higher $\langle n \rangle$ of 10 with a $g^{(2)}(0)$ of 0.21. The modeled response recreates the Rabi oscillations observed for $\langle n \rangle$ of 10 as shown by the solid blue line. (b) The coherence is measured using a Fabry-Perot etalon with an instrument response function (IRF) shown by the solid red line (see Methods). Colored dots represent the measured response. Incoherent emission is observed for higher $\langle n \rangle$ where the reflected signal consists of emission that is far detuned from the input drive frequency, $\Delta\omega \sim 2.5\,\mathrm{GHz}$ for $\langle n \rangle$ of 10 (blue dots). A reduction in incoherent emission with lower incident drive is clearly observed. Note that the incoherent components for $\langle n \rangle$ of 0.001 cannot be separated from the coherent emission as a Voigt fit (orange line) to the raw data gives a similar linewidth to the IRF.

Supplementary Files

This is a list of supplementary files associated with this preprint. Click to download.

- ResonantReflectionSI.pdf